expiration is needed to measure FVC. Patients with back pain can perform slow inspiration and expiration, but rapid inspiration and expiration are not possible. We therefore consider that FVC is more sensitive than vital capacity when comparing restrictive lung function between pre- and post-PVP.

The present study displayed several limitations. The first is the lack of a control group. Patients who develop acute compression fractures are more likely to display decreased lung function, and as these fractures heal, pulmonary function would likely improve. Second, because of the retrospective nature of this study, the number of patients in whom respiratory function was assessed soon after PVP was low.

In conclusion, although the most important goal of PVP is to alleviate pain, the present study clarified that PVP also improves decreased lung function. Such improvements could lower the incidence of pulmonary complications, thus increasing the clinical significance of PVP.

References

1. Gold D. The clinical impact of vertebral fractures: quality of life in woman with osteoporosis. Bone 1996; 18 Suppl 3:185S–9S.
2. Leech JA, Dulberg C, Lellie S, Pattee L, Gay J. Relationship of lung function to severity of osteoporosis in women. Am Rev Respir Dis 1990;141:68–71.
3. Schlaich C, Minne HW, Bruckner T, Wagner G, Gebest HJ, Grunze M, et al. Reduced pulmonary function in patients with spinal osteoporotic fractures. Osteoporosis Int 1998;8:261–7.
4. Cooper C, Atkinson EJ, Jacobsen SJ, O'Fallon WM, Melton LJ. Population-based study of survival after osteoporotic fractures. Am J Epidemiol 1993;137: 1001–5.
5. Galibert P, Deramond H, Rosat P, Le Gars D. Preliminary note on the treatment of vertebral angioma by percutaneous acrylic vertebroplasty. [In French] Neurochirugie 1987;33:166–8.
6. Evans AJ, Jensen ME, Kip KE, DeNardo AJ, Lawler GJ, Negin GA, et al. Vertebral compression fractures: pain reduction and improvement in functional mobility after percutaneous polymethylmethacrylate vertebroplasty – retrospective report of 245 cases. Radiology 2003;226:366–72.
7. Hodler J, Peck D, Gilula LA. Midterm outcome after vertebroplasty: predictive value of technical and patients-related factors. Radiology 2003;227:662–8.
8. Mathis JM, Barr JD, Belkoff SM, Barr MS, Jensen ME, Deramond H. Percutaneous vertebroplasty: a developing standard of care for vertebral compression fractures. Am J Neuroradiol 2001;22:373–81.
9. Calmes V, Vallee JN, Rose M, Chiras J. Osteoblastic and mixed spinal metastases: evaluation of the analgesic efficacy of percutaneous vertebroplasty. Am J Neuroradiol 2007;28:570–4.
10. Kallmes DF, Jensen ME. Percutaneous vertebroplasty. Radiology 2003;229:27–36.
11. Serra L, Kermani FM, Panagiotopoulos K, De Rosa V, Vizioli L. Vertebroplasty in the treatment of osteoporotic vertebral fractures: results and functional outcome in a series of 175 consecutive patients. Minim Invasive Neurosurg 2007;50:12–7.
12. American Thoracic Society. Standardization of spirometry. Am Rev Respir Dis 1987;136:1285–98.
13. Hiwatashi A, Moritani T, Numaguchi Y, Westesson PL. Increase in vertebral body height after vertebroplasty. Am J Neuroradiol 2003;24:185–9.
14. Teng MM, Wei CJ, Wei LC, Luo CB, Lirng JF, Chang FC, et al. Kyphosis correction and height restoration effects of percutaneous vertebroplasty. Am J Neuroradiol 2003;24:1893–900.
15. Carlier RY, Gordji H, Mompoint DM, Vernhet N, Feydy A, Vallee C. Osteoporotic vertebral collapse: percutaneous vertebroplasty and local kyphosis correction. Radiology 2004;233:891–8.

Cardiovasc Intervent Radiol (2008) 31:1174–1177
DOI 10.1007/s00270-008-9325-5

CLINICAL INVESTIGATION

Intraosseous Venography with Carbon Dioxide in Percutaneous Vertebroplasty: Carbon Dioxide Retention in Renal Veins

Atsushi Komemushi · Noboru Tanigawa · Shuji Kariya · Hiroyuki Kojima · Yuzo Shomura · Takanori Tokuda · Motoo Nomura · Jiro Terada · Minoru Kamata · Satoshi Sawada

Received: 15 January 2008 / Accepted: 28 February 2008 / Published online: 21 March 2008

Abstract The objective of the present study was to determine the frequency of gas retention in the renal vein following carbon dioxide intraosseous venography in the prone position and, while citing references, to examine its onset mechanisms. All percutaneous vertebroplasties performed at our hospital from January to December 2005 were registered and retrospectively analyzed. Of 43 registered procedures treating 79 vertebrae, 28 procedures treating 54 vertebrae were analyzed. Vertebral intraosseous venography was performed using carbon dioxide as a contrast agent in all percutaneous vertebroplasty procedures. In preoperative and postoperative vertebral CT, gas retention in the renal vein and other areas was assessed. Preoperative CT did not show gas retention (0/28 procedures; 0%). Postoperative CT confirmed gas retention in the renal vein in 10 of the 28 procedures (35.7%). Gas retention was seen in the right renal vein in 8 procedures (28.6%), in the left renal vein in 5 procedures (17.9%), in the left and right renal veins in 3 procedures (10.7%), in vertebrae in 22 procedures (78.6%), in the soft tissue around vertebrae in 14 procedures (50.0%), in the spinal canal in 12 procedures (42.9%), and in the subcutaneous tissue in 5 procedures (17.9%). In conclusion, in our study, carbon dioxide gas injected into the vertebra frequently reached and remained in the renal vein.

Keywords Interventional radiology · Vertebroplasty · Carbon dioxide · Intraosseous venography · Spine

A. Komemushi (✉) · N. Tanigawa · S. Kariya · H. Kojima · Y. Shomura · T. Tokuda · M. Nomura · J. Terada · M. Kamata · S. Sawada
Department of Radiology, Kansai Medical University, 2-3-1 Shinmachi, Hirakata, Osaka 573-1191, Japan
e-mail: kome64@yo.rim.or.jp

Introduction

The use of intraosseous venography in percutaneous vertebroplasty remains controversial [1–6]. Intraosseous venography enables determination of whether a needle tip is inside the vertebra, whether a needle communicates with the intravertebral clefts, and macroscopic movements of bone fragments; demonstrates direct filling of veins leading to the epidural space without first passing through bone and intertrabecular spaces; and demonstrates the extravertebral pathway of contrast medium leakage. On the other hand, the disadvantages associated with intraosseous venography are that residual positive contrast medium in the vertebra hinders bone cement injection when there is a difference in viscosity between contrast medium and bone cement, and the flow of bone cement cannot be predicted [3–6]. When performing percutaneous vertebroplasty, we use carbon dioxide, a negative contrast medium, in intraosseous venography [1]. While the imaging ability of carbon dioxide is inferior to that of nonionic positive contrast media, because carbon dioxide is a negative contrast medium, it does not hinder bone cement injection if it remains in the vertebra.

Following carbon dioxide intraosseous venography in the prone position, when CT is performed postoperatively to determine the distribution of bone cement, we have sometimes seen gas retention in the renal vein. To the best of our knowledge, there have been no reports of gas retention in the renal vein following carbon dioxide venography. The objective of the present study is to determine the frequency of gas retention in the renal vein following carbon dioxide intraosseous venography in the prone position and, while citing references, to examine its onset mechanisms.

Materials and Methods

All percutaneous vertebroplasties performed at our hospital from January to December 2005 were registered and retrospectively analyzed. The total number of all percutaneous vertebroplasty procedures in this period was 43. Preoperative vertebral CT was performed to determine puncture route, postoperative vertebral CT was performed to confirm bone cement distribution, and procedures where the left and right renal hilar regions were depicted were chosen for further analysis. Of 43 registered procedures treating 79 vertebrae, 28 procedures treating 54 vertebrae (Th7, 1; Th11, 5; Th12, 10; L1, 13; L2, 12; L3, 11; L4, 2; and L5, 1) were analyzed. All procedures included at least one vertebra from Th12 to L3.

Percutaneous vertebroplasties were performed using an IVR-CT system (Advantx-ACT; GE Medical Systems, Milwaukee, WI, USA), which is a combination of angiographic equipment and CT equipment on a single fluoroscopy table. After intramuscular injection of 25 mg of hydroxyzine hydrochloride (Atarax P; Pfizer Japan Inc., Tokyo), 0.5 mg of atropine sulfate (Tanabe Seiyaku Co., Ltd., Osaka, Japan) and 10 mg of morphine hydrochloride (Sankyo Co., Ltd., Tokyo), the patient was positioned prone on the fluoroscopy table. Preoperative vertebral CT was performed in order to reference the puncture site and angle. The skin overlying the vertebral body to be injected was cleaned and draped. The skin, subcutaneous tissues, and periosteum over the pedicle to be punctured were then anesthetized with 1% lidocaine hydrochloride (Xylocaine polyamp, 1%; AstraZeneca KK, Osaka, Japan) using a 22 G × 70-mm Cathelin Needle (Terumo Europe N.V., Leuven, Belgium), with reference to CT images and lateral fluoroscopic guidance, and the needle tip was retained adjacent to the pedicle. CT was then performed to confirm the needle location. Using the needle as a guide, a 13-G needle (Osteo-site Bone Biopsy Needle Murphy M2; length, 10 cm; Cook Inc., Bloomington, IN, USA) was advanced without fluoroscopic guidance until its tip penetrated the cortex. CT was again performed to verify the needle position. Under lateral fluoroscopic guidance, the needle was then advanced into the vertebral body. Ideally, the tip of the needle was placed in the anterior third of the vertebral body, close to the midline. More posterior needle positions occasionally had to be accepted when treating severely compressed vertebral bodies with steep pedicle angulation.

Venography was then performed using carbon dioxide (CO_2) as a contrast agent. CO_2 was drawn from a CO_2 generator through a sterile filter into a 10- or 20-ml syringe (Gaster; Asahi Keiki Co., Osaka, Japan). After connecting the syringe containing CO_2 to the bone biopsy needle via 50 cm of extensible tubing, the operator manually injected CO_2 while keeping as far from the fluoroscopic field as possible. Frontal and lateral venograms were obtained using digital subtraction angiography (DSA). The amount of CO_2 used in venography was 10 ml for thoracic and 20 ml for lumbar vertebrae [1].

After this, 20 g of methylmethacrylate powder (Osteobond copolymer bone cement; Zimmer, Warsaw, IN, USA) was mixed with 5 g of dry heat-sterilized barium sulfate powder (Horii Pharmaceutical Ind., Ltd., Osaka, Japan) to increase its opacity [7]. Next, 10 ml of liquid methylmethacrylate monomer was added to the powder, and the resulting polymethylmethacrylate (PMM) mixture was blended to a toothpaste-like consistency. The PMM was loaded into a 10-ml syringe (Terumo Corp., Tokyo) and then backfilled into screw-type 1-ml syringes or the Bone Cement Injector system, ensuring that air was expelled from the PMM.

The PMM was injected under lateral fluoroscopic guidance. Injection was terminated when adequate filling of the vertebral body was achieved or when leakage outside the vertebral body occurred. When leakage occurred, the needle was repositioned and additional PMM was injected to fill the remaining part of the vertebral body. The needle was then removed, and postoperative vertebral CT was performed to confirm PMM distribution. After the CT procedure, all patients were observed in the supine position for 2 h.

In preoperative and postoperative vertebral CT, gas retention in the renal vein and other areas was assessed.

Results

Preoperative CT did not show gas retention (0/28 procedures: 0%).

Postoperative CT confirmed gas retention in the renal vein in 10 of the 28 procedures (35.7%). Gas retention was seen in the right renal vein in 8 of the 28 procedures (28.6%), in the left renal vein in 5 of the 28 procedures (17.9%), and in the left and right renal veins in 3 of the 28 procedures (10.7%) (Fig. 1).

With regard to gas retention in areas beside the renal vein, gas retention was seen in vertebrae in 22 of the 28 procedures (78.6%), in the soft tissue around vertebrae in 14 of the 28 procedures (50.0%), in the spinal canal in 12 of the 28 procedures (42.9%), and in the subcutaneous tissue in 5 of the 28 procedures (17.9%) (Table 1).

Discussion

When carbon dioxide, a negative contrast medium, is used for intraosseous venography during percutaneous

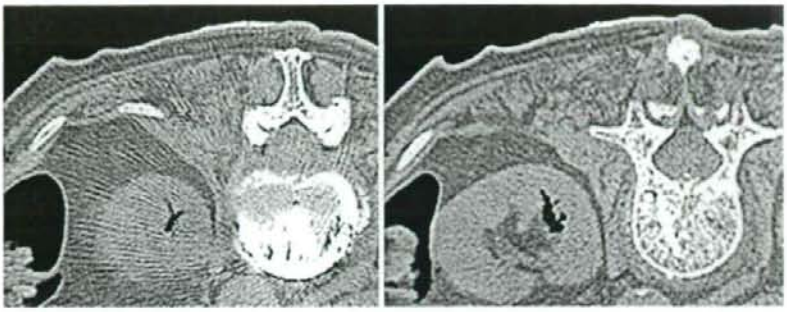

Fig. 1 CT images following carbon dioxide intraosseous venography in the prone position

Table 1 Locations where gas retention in the renal veins was seen (n = 28 procedures)

	Right renal hilus	Left renal hilus	Inside vertebra	Soft tissue around vertebra	Inside spinal tube	Subcutaneous tissue
Preoperative CT	0	0	0	0	0	0
Postoperative CT	8 (28.6%)	5 (17.9%)	22 (78.6%)	14 (50.0%)	12 (42.9%)	5 (17.9%)

vertebroplasty, even if the contrast medium remains inside the vertebra, bone cement injection is not hindered. We have observed gas retention in the renal hilus following carbon dioxide intraosseous venography. To the best of our knowledge, there have been no reports of gas retention in the renal hilus following carbon dioxide intraosseous venography. In the present study, we investigated the frequency of gas retention in the renal hilus following carbon dioxide intraosseous venography in the prone position; and CT after intraosseous venography showed gas retention in the renal vein in 10 of the 28 procedures (35.7%).

Carbon dioxide injected into the vertebra travels to extravertebral veins via the basivertebral veins. On the dorsal side of the vertebra, the basivertebral veins communicate with the anterior internal vertebral venous plexus on the anterior surface of the spinal canal, and on the ventral side of the vertebra, the basivertebral veins communicate with the anterior external vertebral venous plexus on the anterior surface of the vertebra. These venous plexuses communicate with the inferior vena cava via the intercostal and lumbar veins, and the anterior external vertebral venous plexus communicates directly with the inferior vena cava [8]. As the renal vein communicates with the lumbar veins and inferior vena cava, carbon dioxide gas injected in the vertebra reaches the renal vein via these pathways. These pathway veins are characterized by a lack of venous valves, thin walls, and easily altered flow [9].

Carbon dioxide tends to travel upward [10]. As the kidney is located on the dorsal side of the trunk in the superior direction, the prone position allows the carbon dioxide to travel to the renal vein. In addition, because the viscosity of carbon dioxide is low, it can easily flow backward through vessels [10].

When performing carbon dioxide intraosseous venography in the prone position, the frequency of gas retention in the renal vein was relatively high, at 35.7%; this is because there are communicating vessels from the spine to the renal vein, the prone position allows carbon dioxide to travel to the kidney, and the low viscosity of carbon dioxide increases the likelihood of backward flow through the veins.

Bone cement leakage is an important complication of percutaneous vertebroplasty. When injecting bone cement into the vertebra, cement leakage into a vein can cause an embolus. Chung et al. reported cement embolization of the renal vein as an extremely rare complication of percutaneous vertebroplasty, but its onset mechanism has not been clarified [11]. In our study, carbon dioxide gas injected into the vertebra frequently reached and remained in the renal vein. Because bone cement differs from carbon dioxide in terms of viscosity and specific gravity, renal vein embolization due to bone cement is thought to be rare. The present study may aid in the clarification of the onset mechanisms of renal vein embolization due to bone cement, which is a rare complication of percutaneous vertebroplasty.

References

1. Tanigawa N, Komemushi A, Kariya S et al (2005) Intraosseous venography with carbon dioxide contrast agent in percutaneous vertebroplasty. AJR 184:567–570
2. Jansen ME, Evans AJ, Mathis JM et al (1997) Percutaneous polymethylmethacrylate vertebroplasty in the treatment of osteoporotic vertebral body compression fractures: technical aspect. Am J Neuroradiol 18:1897–1904
3. McGraw JK, Heatwole EV, Strnad BT et al (2002) Predictive value of intraosseous venography before percutaneous vertebroplasty. J Vasc Interv Radiol 13:149–153

4. Gaughen JR Jr, Jensen ME, Schweickert PA et al (2002) Relevance of antecedent venography in percutaneous vertebroplasty for the treatment of osteoporotic compression fractures. Am J Neuroradiol 23:594–600
5. Vasconcelos C, Gailloud P, Beauchamp NJ et al (2002) Is percutaneous vertebroplasty without pretreatment venography safe? Evaluation of 205 consecutives procedures. Am J Neuroradiol 23:913–917
6. Peh WC, Gilula LA (2003) Additional value of a modified method of intraosseous venography during percutaneous vertebroplasty. AJR 180:87–91
7. Leibold RA, Gilula LA (2002) Sterilization of barium for vertebroplasty: an effective, reliable, and inexpensive method to sterilize powders for surgical procedures. AJR 179:198–200
8. Groen RJ, du Toit DF, Phillips FM et al (2004) Anatomical and pathological considerations in percutaneous vertebroplasty and kyphoplasty: a reappraisal of the vertebral venous system. Spine 29:1465–1471
9. Baston OV (1940) The function of the vertebral veins and their role in the spread of metastases. Arch Surg 112:138–149
10. Hawkins IF, Caridi JG (1998) Carbon dioxide (CO_2) digital subtraction angiography: 26-year experience at the University of Florida. Eur Radiol 8:391–402
11. Chung SE, Lee SH, Kim TH et al (2006) Renal cement embolism during percutaneous vertebroplasty. Eur Spine J Suppl 5:590–594

Corpus Callosum in Patients with Obsessive-Compulsive Disorder: Diffusion-Tensor Imaging Study[1]

Yukiko Saito, MD
Kenji Nobuhara, MD, PhD
Gaku Okugawa, MD, PhD
Katsunori Takase, MD, PhD
Tatsuya Sugimoto, MD
Mami Horiuchi, MD
Chiho Ueno, MD
Minoru Maehara, MD
Naoto Omura, MD
Hiroaki Kurokawa, MD, PhD
Koshi Ikeda, MD, PhD
Noboru Tanigawa, MD, PhD
Satoshi Sawada, MD, PhD
Toshihiko Kinoshita, MD, PhD

Purpose: To prospectively examine microstructural white matter abnormalities in the corpus callosum (CC) of patients with obsessive-compulsive disorder (OCD), as compared with control subjects, and to investigate the relationship between diffusion-tensor (DT) imaging measures of the CC region and clinical symptoms of OCD.

Materials and Methods: Institutional review board approval was obtained, and each participant—or the participant's parent(s)—provided written informed consent. Sixteen patients with OCD (seven male, nine female; mean age, 28.7 years ± 9.8 [standard deviation]) and 16 matched healthy volunteers (control subjects) (seven male, nine female; mean age, 29.9 years ± 9.0) were examined. Mean diffusivity and fractional anisotropy (FA) were measured in five subdivisions of the CC. The paired *t* test was performed to compare the mean diffusivity or the FA in CC regions between the patients with OCD and the control subjects.

Results: There were no significant differences (rostrum, $P = .15$; genu, $P = .88$; rostral body, $P = .12$; isthmus, $P = .77$; splenium, $P = .88$) in mean diffusivity between the patients with OCD and the healthy volunteers. A significant reduction in FA was observed in the rostrum of the CC in patients with OCD compared with the rostral FA in the control subjects ($P < .001$). Higher FA in only the rostrum correlated significantly with lower Yale-Brown obsessive-compulsive scale score ($r = -0.72$, $P = .002$).

Conclusion: Study results support the widely held view that the orbital prefrontal region is involved in the pathophysiology of OCD and indicate that the orbitofrontal circuit influences symptom severity in patients with OCD.

[1] From the Departments of Neuropsychiatry (Y.S., K.N., G.O., K.T., T.S., M.H., C.U., T.K.) and Radiology (Y.S., M.M., N.O., H.K., K.I., N.T., S.S.), Kansai Medical University, 10-15 Fumizono-cho, Moriguchi City, Osaka, 570-8506, Japan. Received August 23, 2006; revision requested October 30; revision received March 2, 2007; accepted March 21; final version accepted July 5. Supported by grant 16591173 from the Ministry of Education Science and Culture of Japan. **Address correspondence to** Y.S. (e-mail: *saitoyu@takii.kmu.ac.jp*).

Obsessive-compulsive disorder (OCD) is characterized by intense, intrusive, and unwanted thoughts or ideas in association with urges to perform ritualistic behaviors (1). OCD is often chronically disabling, with concomitant impairments in interpersonal and occupational function, and patients with this disorder report having senseless and unpleasant symptoms (2). Obsessions and compulsions typically emerge around the 2nd to 3rd decade of life and often are resistant to psychodynamic therapeutic approaches; however, they are quite responsive to pharmacologic intervention (3).

Neuropsychologic studies have revealed cognitive impairments with OCD (4,5). The corpus callosum (CC), the largest interhemispheric white matter commissure connecting the cerebral hemispheres, has a crucial role in interhemispheric communication and cognitive processes (6). The subdivisions of the CC may be roughly associated with various cortical regions, although there is considerable overlap. The possibility of topographic organization of callosal fibers is based on experimental work with monkeys (7), autoradiographic study results (8,9), and clinical study results (10,11). The rostrum contains fibers from the orbitofrontal cortex (OFC), and the genu connects the lateral and medial surfaces of the frontal lobes. The body of the CC connects wide neocortical homotopic regions of the cerebral hemispheres, including the premotor, supplementary motor, motor, somatesthetic, and posterior parietal regions. The isthmus connects the superior temporal and posterior parietal regions, while the splenium connects the occipital and inferior temporal regions.

Neuroimaging study results have repeatedly implicated the OFC in the pathophysiology of OCD. The OFC, when measured at baseline (12,13) or during exposure (14) to triggering stimuli, is hyperactive in patients with OCD. Substantial reductions in OFC activity have been observed after successful pharmacologic and behavioral therapy (15). The consistency with which OFC hyperactivity has been observed in these studies suggests that the OFC may make a unique contribution to OCD. The OFC is positioned at a point of interface between the sensory association cortices, limbic structures, and subcortical regions involved in controlling the automatic and motor effector pathways (16). Although recent research on OCD has been focused on the neuroanatomic circuitry, including the circuitry in the OFC, the abnormalities of the white matter in the orbitofrontal region in patients with OCD have been examined in only a few studies.

Magnetic resonance (MR) diffusion-tensor (DT) imaging is used to noninvasively examine the molecular diffusion of water in vivo and to directly appreciate the anatomic integrity of neural fibers (axons and myelin) in white matter. Thus, DT imaging yields information about white matter tracts and their organization (17). Specifically, it yields an index of microstructural integrity through quantification of the magnitude and directionality of restricted tissue water mobility (diffusion anisotropy) in three dimensions. The magnitude and directionality are evaluated specifically by using measurements of mean diffusivity (D_M), a measure of the magnitude of diffusion, and fractional anisotropy (FA), a measure of the directionality of diffusion. DT imaging has been used successfully to evaluate the white matter fiber integrity in patients with psychiatric diseases such as schizophrenia (18–20) and depression (21).

We hypothesized that OCD is associated with white matter integrity abnormalities in the orbitofrontal brain region. Thus, the purpose of our study was to prospectively examine the microstructural white matter abnormalities in the CC of patients with OCD, as compared with healthy control subjects, and to investigate the relationship between DT measures of the CC region and clinical symptoms of OCD.

Advance in Knowledge

- In patients with obsessive-compulsive disorder (OCD), we observed abnormal white matter anisotropy in the rostrum of the corpus callosum (CC) and an inverse relationship between white matter anisotropy in the CC rostrum and severity of OCD symptoms.

Implication for Patient Care

- Diffusion-tensor imaging performed in addition to Yale-Brown obsessive-compulsive scale scoring may help to predict the severity of OCD symptoms.

Materials and Methods

Patients

The study protocol was approved by our institutional review board, and written informed consent was obtained from all patients or their parents, depending on the age of the patient. All patients had received a diagnosis of OCD based on criteria listed in the fourth edition of the *Diagnostic and Statistical Manual of Mental Disorders* (DSM-IV) (22). Between April 2004 and October 2005, 18 consecutive patients with OCD who met

Published online before print
10.1148/radiol.2462061469

Radiology 2008; 246:536–542

Abbreviations:
CC = corpus callosum
D_M = mean diffusivity
DT = diffusion tensor
FA = fractional anisotropy
HDRS = Hamilton Depression Rating Scale
OCD = obsessive-compulsive disorder
OFC = orbitofrontal cortex
ROI = region of interest
STIR = short inversion time inversion recovery
Y-BOCS = Yale-Brown Obsessive-Compulsive Scale

Author contributions:
Guarantors of integrity of entire study, Y.S., K.N.; study concepts/study design or data acquisition or data analysis/interpretation, all authors; manuscript drafting or manuscript revision for important intellectual content, all authors; manuscript final version approval, all authors; literature research, Y.S., K.N., G.O., H.K., K.I.; clinical studies, Y.S., K.N., G.O., K.T., T.S., C.U., H.K., K.I.; statistical analysis, Y.S., K.N., G.O.; and manuscript editing, all authors

Authors stated no financial relationship to disclose.

our study criteria were recruited for this investigation at our university hospital. We excluded patients who *(a)* had cardiac pacemakers, metallic clips, or other metallic implants or artifacts in their bodies; *(b)* had substantial medical illness or neurologic (eg, Tourette syndrome, Huntington disease, and Parkinson disease), pulmonary, cardiac, renal, hepatic, endocrine, or metabolic disorders; *(d)* had DSM-IV–defined dementia, delirium, schizophrenia, schizoaffective disorder, delusional disorder, brief reactive psychosis, or psychotic disorders not otherwise specified; *(e)* had DSM-IV–defined mental retardation; *(f)* had lacunar infarcts; *(g)* were currently or previously dependent on or abusers of DSM-IV–defined alcoholic or psychoactive substances; and/or *(h)* were pregnant. All patients with lacunar infarcts in any location were excluded. Thus, two patients found to have lacunar infarction were excluded from our study. The final study cohort included 16 patients (seven male, nine female; age range, 16–47 years; mean age, 28.7 years ± 9.8 [standard deviation]).

The final study cohort of 16 patients had a mean total Yale-Brown Obsessive-Compulsive Scale (Y-BOCS) score of 26.0 ± 5.3, and their mean scores on the obsessive and compulsive subscales were 14.6 ± 3.5 and 11.4 ± 2.8, respectively. Their mean Hamilton Depression Rating Scale (HDRS) score was 5.3 ± 2.7. No patients had comorbid disorders such as major depression or panic disorder. Ten patients had doubting obsessions (wondering whether something was done) in association with checking compulsions (checking that it was done), whereas six patients had contamination obsessions (fear of germs) in association with washing compulsions.

All but three patients were receiving medication for their OCD symptoms at the time of the MR examination: Five patients were taking paroxetine hydrochloride only; two patients, a combination of paroxetine hydrochloride and benzodiazepines; and two patients, a combination of fluvoxamine maleate and benzodiazepines. One patient each was taking a combination of paroxetine hydrochloride, fluvoxamine maleate, and benzodiazepines; a combination of paroxetine hydrochloride and clomipramine hydrochloride; a combination of fluvoxamine maleate, benzodiazepines, and sulpiride; or a combination of fluvoxamine maleate, milnacipran hydrochloride, and benzodiazepines.

Control Subjects

Sixteen healthy volunteers (seven male, nine female; age range, 16–47 years; mean age, 29.9 years ± 9.0) matched one-to-one in age, sex, and handedness with the patients who had OCD participated in the study as control subjects after giving informed consent. Institutional review board approval was also obtained to examine these volunteers. Neither these volunteers nor their first-degree relatives had a history of psychiatric illness. They underwent MR imaging of the brain and were subsequently confirmed to have normal MR findings and no neurologic deficits at clinical examination.

Clinical Assessments

Only the 16 patients with OCD were examined with the Y-BOCS and the 17-item HDRS. Greater symptom severity results in higher Y-BOCS and HDRS scores. Both assessments were performed by one trained psychiatrist (Y.S., 5 years experience in psychiatry) at the initial visit, 2 weeks before the MR examinations.

MR Imaging Protocol

The MR examinations were performed with a 1.5-T unit (Signa Horizon LX; GE Medical Systems, Milwaukee, Wis). Head motion was minimized with restraining pads and tape before imaging. Echo-planar MR images were obtained in the patients with OCD and the control subjects and were checked for head motion. Sagittal short inversion time inversion-recovery (STIR) echo-planar images were acquired first, with a section clearly showing the anterior and posterior commissures. The superoinferior thickness of the rostrum in the sagittal plane was measured. Then, a series of transverse diffusion-weighted images with a diffusion-sensitizing gradient (b = 1000 sec/mm^2) were obtained. Diffusion was measured along six noncolinear directions. We used single-shot spin-echo echo-planar sequences for DT analysis. All acquisitions were performed parallel to the anterior commissure–posterior commissure line with use of the following parameters: >17 000/>115.6 (repetition time msec/echo time msec), 128 × 128 matrix, 24 × 24-cm field of view, four signals acquired, 4.0-mm section thickness, and no intersection gap.

The diffusion-weighted images were transferred to a dedicated workstation (Sun Microsystems, Santa Clara, Calif), where the DT data were postprocessed by using Functool 2.2.49 software (GE Medical Systems). Echo-planar image distortion was corrected. The first step of this procedure entails correcting the distortions usually induced by the eddy current related to the large diffusion-sensitizing gradients. This correction algorithm is based on the maximization of mutual information to estimate the three parameters of a geometric distortion model inferred from the acquisition principle. The second step of the procedure involves replacing the standard least squares–based approach with the Geman-McLure M estimator approach to eliminate outlier-related artifacts.

D_M and FA maps were then computed by using the DT data. The Functool software applies thresholding to apparent diffusion coefficient maps that may substantially affect mean region-of-interest (ROI) data. We were aware of this and took care to avoid it.

Diffusion eigenvectors and eigenvalues (λ_1, λ_2, and λ_3), which correspond to the main diffusion direction and the associated diffusivity, were calculated from the DT data. FA values, which yield information about the degree of diffusion anisotropy in white matter, and D_M values, which yield information about the magnitude of diffusion, were then calculated:

$$FA = \sqrt{\frac{3}{2}} \cdot \frac{\sqrt{(\lambda_1 - \lambda)^2 + (\lambda_2 - \lambda)^2 + (\lambda_3 - \lambda)^2}}{\sqrt{\lambda_1^2 + \lambda_2^2 + \lambda_3^2}}$$

and

$$D_M = (\lambda_1 + \lambda_2 + \lambda_3)/3.$$

ROI Selection and Analysis

The CC was clearly delineated in the midsagittal plane on the STIR brain MR images. The lack of anatomic landmarks on the midsagittal view of the CC made it difficult to define the corresponding cortical areas from which the fibers originate. Thus, seven callosal subdivisions were defined on the basis of the scheme of regional divisions of the CC proposed by Witelson and Kigar (23) (Fig 1a). We investigated the plane parallel to the anterior commissure–posterior commissure plane, including each subdivision of the CC, on the sagittal STIR images (Fig 1b). Each ROI consisted of manually traced 2-mm squares placed over the anatomic horizontal T2-weighted imaging plane, which was determined on the basis of the sagittal STIR image findings. The borderlines between the anterior middle and posterior middle bodies of the CC were not clearly defined in the transverse T2-weighted imaging planes. Therefore, the following five subdivisions of the CC were chosen as ROIs: the rostrum, genu, rostral body, isthmus, and splenium (Fig 2).

Two trained physicians (Y.S., K.N.) conducted all FA measurements in consensus. These physicians have 5 (Y.S.) and 10 (K.N.) years experience in brain MR imaging research. They were blinded to the subject group when they performed the ROI analysis. For each subject, the ROIs were transferred onto FA maps and the FA was calculated for each selected CC ROI. The interoperator reliability between the two physicians in assessing the DT measures in 10 randomly selected subjects (five patients with OCD, five healthy volunteers) was also confirmed.

Statistical Analyses

The two physicians (Y.S., K.N.) were blinded to information about the images that they were analyzing. Interoperator reliability in assessing the DT measures was confirmed by using intraclass correlation coefficients. Data for 10 participants (five patients with OCD, five healthy volunteers) collected by one psychiatrist (K.N.) were used to compare the patient and control subject data. Mean DT values for each ROI, including 95% confidence intervals for the difference in mean values between

Figure 1

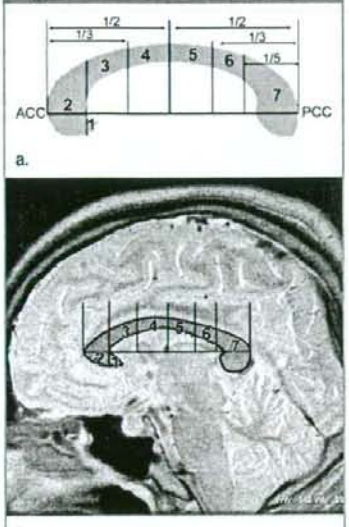

Figure 1: Regional subdivisions of CC in adult human based on **(a)** regional division scheme of the CC and **(b)** corresponding sagittal STIR MR image findings (3000/8.8/100 [repetition time msec/echo time msec/inversion time msec]). Anterior CC *(ACC)* and posterior CC *(PCC)* are extreme anterior and extreme posterior points of the CC, respectively, with anterior CC–posterior CC distance defined as the length of the CC. Anterior CC–posterior CC distance is used as linear axis to subdivide CC into anterior and posterior halves; anterior, middle, and posterior thirds; and posterior fifth region, which is roughly congruent with the splenium (region *7*). Line perpendicular to axis at extreme anterior point on inner convexity of anterior CC is used to define rostrum (region *1*) and extreme anterior division of CC, which is roughly congruent with the genu (region *2*). Region *3*, the rostral body, is defined as anterior third of CC minus regions *1* and *2*. Region *4*, the anterior middle body, is defined as anterior half minus anterior third. Region *5*, the posterior middle body, is defined as posterior half minus posterior third. Region *6*, the isthmus, is defined as posterior third minus posterior fifth. Regions *3–6* constitute CC body.

Figure 2

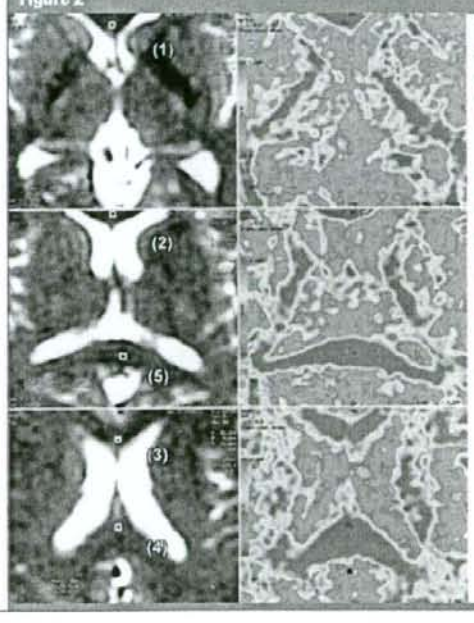

Figure 2: Transverse T2-weighted MR images (left, $b = 0$ sec/mm^2) and corresponding FA maps (right, $b = 1000$ sec/mm^2) in patient with OCD (>17 000/>115.6, 4-mm section thickness). ROIs are drawn in rostrum *(1)*, genu *(2)*, rostral body *(3)*, isthmus *(4)*, and splenium *(5)* of CC. Right: Colors, demonstrated by using Functool 2.2.49 software, indicate various grades of white matter anisotropy. Blue indicates low grade of white matter anisotropy, and red indicates high grade of white matter anisotropy.

the two groups (patients with OCD vs healthy volunteers), were calculated. The paired *t* test was used to compare DT values for the CC regions between the patients with OCD and the matched control subjects. Because five comparisons were performed for each DT measure, *P* values lower than .01 were considered significant on the basis of Bonferroni correction. The correlations between DT measures of the CC regions studied and Y-BOCS and HDRS scores were investigated by using Spearman rank correlation coefficients. All statistical analyses were performed by using SPSS statistical software (SPSS for Windows, release 11.5 J; SPSS, Chicago, Ill).

Results

Our check of the raw echo-planar images for head motion revealed that the patients with OCD and the control subjects had kept equally still. The average superoinferior thickness of the rostrum measured in the sagittal plane for both groups was 6.875 mm. All intraclass correlation coefficients of DT measures were greater than 0.89 for every ROI, indicating excellent interoperator reliability.

There were no significant differences in D_M between the patients with OCD and the healthy volunteers (Table 1). A significant reduction in FA was observed in the CC rostrum of the patients with OCD compared with the rostral FA in the control subjects ($P < .001$). FA in the other subdivisions did not differ significantly between the patients and the healthy volunteers (Table 2). Higher FA in only the rostrum correlated significantly with lower Y-BOCS score ($r = -0.72$, $P = .002$) (Fig 3). HDRS score did not correlate with FA in the rostrum ($r = 0.06$, $P = .84$). Because none of the patients with OCD had an HDRS score higher than 7, we found noncorrelation between HDRS score and FA in the rostrum.

Discussion

Our study results indicate that in patients with OCD, there is abnormal white matter anisotropy in the rostrum of the CC and an inverse relationship between white matter anisotropy in the CC rostrum and severity of OCD symptoms. The reduced white matter anisotropy observed in our study suggests that patients with OCD possibly have microstructural abnormalities in the CC rostrum itself and fiber integrity abnormalities in the orbital prefrontal region that contains fibers extending into the rostrum. There is a large amount of experimental and clinical evidence that the OFC is involved in the mediation of emotional responses to biologically important stimuli (16). Results of animal studies suggest that hoarding, a common OCD symptom, is mediated by the ventromedial striatum, globus pallidus, and medial dorsal thalamus—all of which are connected to the OFC (16,24). Thus, heightened OFC activity may make individuals with OCD particularly efficient at recognizing conditioned aversive reinforcers and more vulnerable to anticipatory anxiety or distress (25). Since the OFC is involved in maintaining representations of the

Table 1

Mean Diffusivity for Selected Regions in Patients with OCD and Healthy Volunteers

Region	Mean Diffusivity*		*P* Value†	95% Confidence Interval‡
	Patients with OCD	Healthy Volunteers		
Rostrum	8.90 ± 2.28	7.74 ± 1.15	.15	−0.46, 2.78
Genu	8.10 ± 1.12	8.15 ± 1.01	.88	−0.88, 0.77
Rostral body	8.57 ± 1.32	7.93 ± 0.72	.12	−1.75, 1.44
Isthmus	9.09 ± 1.24	8.96 ± 1.00	.77	0.78, 1.04
Splenium	7.14 ± 0.81	7.12 ± 1.08	.88	−0.66, 0.57

* Mean diffusivity values ± standard deviations.

† $P < .01$ indicates significant difference on the basis of Bonferroni correction.

‡ Ninety-five percent confidence intervals for the difference in mean values between the patients and healthy volunteers.

Table 2

Mean FA Values for Selected Regions in Patients with OCD and Healthy Volunteers

Region	Mean FA*		*P* Value†	95% Confidence Interval‡
	Patients with OCD	Healthy Volunteers		
Rostrum	0.55 ± 0.07	0.69 ± 0.06	<.001	−1.18, −0.97
Genu	0.80 ± 0.07	0.81 ± 0.09	.70	−0.53, 0.36
Rostral body	0.68 ± 0.08	0.70 ± 0.06	.46	−0.66, 0.32
Isthmus	0.69 ± 0.08	0.73 ± 0.07	.06	−0.93, 0.01
Splenium	0.87 ± 0.10	0.86 ± 0.08	.74	−0.46, 0.63

* Mean FA values ± standard deviations.

† $P < .01$ indicate significant difference on the basis of Bonferroni correction.

‡ Ninety-five percent confidence intervals for the difference in mean values between the patients and healthy volunteers.

Figure 3

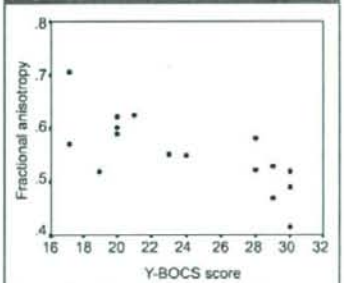

Figure 3: Graph illustrates relationship between Y-BOCS score and FA in CC rostrum of patients with OCD.

reinforcement value of stimuli in working memory, the inability of patients with this disorder to inhibit intrusive thoughts and images may be interpreted as reflective of a hyperactive working memory (26). The correlations between Y-BOCS score and white matter anisotropy of the CC rostrum that we observed suggest that white matter abnormalities in the orbitofrontal region are implicated in OCD symptom severity.

Szeszko et al (27) reported their use of DT imaging in patients with OCD. They compared, voxel by voxel, the imaging data in 15 patients with OCD and 15 healthy volunteers and observed substantially lower FA bilaterally in three areas of the anterior cingulated gyrus white matter in the patients with OCD. In our study, however, we chose an ROI analysis method aimed at identifying microstructural white matter abnormalities of the CC. The cingulum was not clearly defined in the transverse T2-weighted imaging planes, so we could not evaluate it. The contrasting findings of these two DT imaging studies may be due to differences in characteristics, such as age, sex, handedness, race, total Y-BOCS score, and/or HDRS score, between the patient groups. Furthermore, important group differences in the white matter integrity in other brain regions implicated in the pathophysiology of OCD, including the orbitofrontal lobe and striatal regions, were not observed in the Szeszko et al study (27).

We observed abnormal white matter FA in the CC rostrum of the patients with OCD. However, there were no significant differences in D_M between the groups. FA and D_M can be studied independently. FA is a measure of the directionality of diffusion. On the other hand, D_M is a measure of the average diffusion in all directions and thus is more sensitive to fiber density than to fiber orientation and organization (28). Although microstructural changes can be roughly estimated by using FA or D_M, both parameters are indispensable for yielding more pertinent information about morphologic changes in the brain. DT measures can be influenced by many factors, such as dense packing of axons, relative permeability of the membrane to water, internal axonal structure, tissue water content or degree of myelination, and/or the pathophysiology underlying the reduced white matter anisotropy. Although the pathophysiology underlying the reduced white matter anisotropy in the CC rostrum in patients with OCD has not been confirmed, more than one process may be responsible for the FA reduction.

Our study had limitations. A relatively small number of patients and control subjects were examined. There were also a few methodologic concerns. Because of the difficulty in placing ROIs in subcortical regions with no remarkable landmarks, microstructural abnormalities of the white matter tracts connecting the OFC to the rostrum were not directly examined. The Functool software applies thresholding to apparent diffusion coefficient maps that may substantially affect mean ROI data. Thus, the potential effects of medication on DT measures could not be examined. Also, since the source diffusion-weighted images had an in-plane spatial resolution of only 1.9 × 1.9 mm and a thickness of 4 mm, the noise introduced during the conversion of these images to FA maps could have limited the spatial resolution even further. We also cannot exclude the possibility that potential partial volume averaging effects influence DT measurements, especially in such a small subdivision of the CC as the rostrum, whose volume may differ between groups. However, for all subjects, the superoinferior thickness of the rostrum measured in the sagittal plane was 5–9 mm, greater than the 4-mm image section thickness. Furthermore, we cannot exclude the possibility that the head motion resulting from anxiety related to being inside the magnet differed between groups. Therefore, we checked the raw echo-planar images for head motion and verified that the patients with OCD and the control subjects had kept equally still.

In conclusion, our study results support the widely held view that the orbital prefrontal region is involved in the pathophysiology of OCD. It is important that the results also indicate that the OFC influences symptom severity in patients with OCD. Future studies with larger numbers of drug-naïve patients and more complex methods, such as tract tracing for direct examination of the targeted white matter, may help to elucidate the contribution of microstructural white matter changes in the orbitofrontal region to the pathophysiology and outcomes of OCD.

Acknowledgments: We are grateful to the MR imaging group at Kansai Medical University for valuable assistance.

References

1. Weissman MM, Bland RC, Canino GJ; for the Cross National Collaborative Group. The cross national epidemiology of obsessive compulsive disorder. J Clin Psychiatry 1994; 55(suppl):5–10.
2. Rasmussen SA, Eisen JL. The epidemiology and differential diagnosis of obsessive compulsive disorder. J Clin Psychiatry 1992; 53(suppl):4–10.
3. Dougherty DD, Rauch SL, Jenike MA. Pharmacotherapy for obsessive-compulsive disorder. J Clin Psychol 2004;60:1195–1202.
4. Purcell R, Maruff P, Kyrios M, Pantelis C. Cognitive deficits in obsessive-compulsive disorder on tests of frontal-striatal function. Biol Psychiatry 1998;43:348–357.
5. Greisberg S, McKay D. Neuropsychology of obsessive-compulsive disorder: a review and treatment implications. Clin Psychol Rev 2003;23:95–117.
6. Gazzaniga MS. Cerebral specialization and interhemispheric communication: does the corpus callosum enable the human condition? Brain 2000;123:1293–1326.
7. Pandya DN, Karol EA, Heilbronn D. The topographical distribution of interhemispheric projections in the corpus callosum of the rhesus monkey. Brain Res 1971;32: 31–43.
8. Barbas H, Pandya DN. Topography of commissural fibers of the prefrontal cortex in the rhesus monkey. Exp Brain Res 1984;55:187–191.
9. Seltzer B, Pandya DN. The distribution of posterior parietal fibers in the corpus callosum of the rhesus monkey. Exp Brain Res 1983;49:147–150.
10. de Lacoste MC, Kirkpatrick JB, Ross ED. Topography of the human corpus callosum. J Neuropathol Exp Neurol 1985;44:578–591.
11. Abe O, Masutani Y, Aoki S, et al. Topography of the human corpus callosum using dif-

fusion tensor tractography. J Comput Assist Tomogr 2004;28:533–539.

12. Baxter LR Jr, Phelps ME, Mazziotta JC, Guze BH, Schwartz JM, Selin CE. Local cerebral glucose metabolic rates in obsessive-compulsive disorder: a comparison with rates in unipolar depression and in normal controls. Arch Gen Psychiatry 1987;44:211–218.

13. Swedo SE, Schapiro MB, Grady CL, et al. Cerebral glucose metabolism in childhood-onset obsessive-compulsive disorder. Arch Gen Psychiatry 1989;46:518–523.

14. Rauch SL, Jenike MA, Alpert NM, et al. Regional cerebral blood flow measured during symptom provocation in obsessive-compulsive disorder using oxygen 15-labeled carbon dioxide and positron emission tomography. Arch Gen Psychiatry 1994;51:62–70.

15. Baxter LR Jr, Schwartz JM, Bergman KS, et al. Caudate glucose metabolic rate changes with both drug and behavior therapy for obsessive-compulsive disorder. Arch Gen Psychiatry 1992;49:681–689.

16. Zald DH, Kim SW. Anatomy and function of the orbital frontal cortex. I. Anatomy, neurocircuitry, and obsessive-compulsive disorder. J Neuropsychiatry Clin Neurosci 1996; 8:125–138.

17. Basser PJ, Pierpaoli C. Microstructural and physiological features of tissues elucidated by quantitative-diffusion-tensor MRI. J Magn Reson B 1996;111:209–219.

18. Lim KO, Hedehus M, Moseley M, de Crespigny A, Sullivan EV, Pfefferbaum A. Compromised white matter tract integrity in schizophrenia inferred from diffusion tensor imaging. Arch Gen Psychiatry 1999;56:367–374.

19. Minami T, Nobuhara K, Okugawa G, et al. Diffusion tensor magnetic resonance imaging of disruption of regional white matter in schizophrenia. Neuropsychobiology 2003; 47:141–145.

20. Okugawa G, Nobuhara K, Minami T, et al. Subtle disruption of the middle cerebellar peduncles in patients with schizophrenia. Neuropsychobiology 2004;50:119–123.

21. Nobuhara K, Okugawa G, Sugimoto T, et al. Frontal white matter anisotropy and symptom severity of late-life depression: a magnetic resonance diffusion tensor imaging study. J Neurol Neurosurg Psychiatry 2006; 77:120–122.

22. American Psychiatric Association. Diagnostic and statistical manual of mental disorders, 4th ed. Washington, DC: American Psychiatric Association, 2000; 456–462.

23. Witelson SF, Kigar DL. Anatomical development of corpus callosum in humans: a review with reference to sex and cognition. In: Molefese DL, Segalowitz SJ, eds. Brain lateralization in children: development implications. New York, NY: Guilford, 1988; 35–37.

24. Mogenson GJ, Wu M. Disruption of food hoarding by injections of procaine into mediodorsal thalamus, GABA into subpallidal region and haloperidol into accumbens. Brain Res Bull 1988;20:247–251.

25. Zald DH, Kim SW. Anatomy and function of the orbital frontal cortex. II. Function and relevance to obsessive-compulsive disorder. J Neuropsychiatry Clin Neurosci 1996;8: 249–261.

26. Goldman-Rakic PS. Circuitry of primate prefrontal cortex and regulation of behavior by representational memory. In: Plum F, Mountcastle V, eds. Handbook of physiology: the nervous system. Bethesda, Md: American Physiological Society, 1987; 373–417.

27. Szeszko PR, Ardekani BA, Ashtari M, et al. White matter abnormalities in obsessive-compulsive disorder: a diffusion tensor imaging study. Arch Gen Psychiatry 2005;62: 782–790.

28. Kubicki M, Westin CF, Nestor PG, et al. Cingulate fasciculus integrity disruption in schizophrenia: a magnetic resonance diffusion tensor imaging study. Biol Psychiatry 2003;54:1171–1180.

Cardiovasc Intervent Radiol (2008) 31:332–335
DOI 10.1007/s00270-007-9246-8

CLINICAL INVESTIGATION

Biochemical Markers of Bone Turnover in Percutaneous Vertebroplasty for Osteoporotic Compression Fracture

Atsushi Komemushi · Noboru Tanigawa · Shuji Kariya · Hiroyuki Kojima · Yuzo Shomura · Takanori Tokuda · Motoo Nomura · Jiro Terada · Minoru Kamata · Satoshi Sawada

Received: 17 July 2007 / Accepted: 9 November 2007 / Published online: 12 December 2007

Abstract
Purpose To evaluate relationships between biochemical markers of bone turnover, bone mineral density, and new compression fractures following vertebroplasty.
Methods Initially, we enrolled 30 consecutive patients with vertebral compression fractures caused by osteoporosis. Twenty-three of the 30 patients visited our hospital for follow-up examinations for more than 4 weeks after vertebroplasty. The patients were divided into two groups: patients with new fractures (group F) and patients with no new fractures (group N). We analyzed differences in the following parameters between these two groups: serum bone alkaline phosphatase, urinary crosslinked N-telopeptide of type I collagen, urinary deoxypyridinoline, and bone mineral density. Next, the patients were divided into another two groups: patients with higher risk (group H: urinary cross-linked N-telopeptide of type I collagen >54.3 nmol BCE/mmol Cr or urinary deoxypyridinoline >7.6 nmol/mmol Cr, and serum bone alkaline phosphatase <29.0 U/l) and patients with lower risk (group L). We analyzed the difference in the rate of new fractures between these two groups.
Results We identified 9 new fractures in 7 patients. There were no significant differences between groups F and N. We identified 5 new fractures in 3 of the 4 patients in group H, and 4 new fractures in 4 of the 19 patients in group L. There was a significant difference in the rate of new fractures between groups H and L.
Conclusions A combination of high levels of bone resorption markers and normal levels of bone formation markers may be associated with increased risk of new recurrent fractures after percutaneous vertebroplasty.

Keywords Interventional radiology · Osteoporosis · Spine · Vertebral fracture · Vertebroplasty

A. Komemushi (✉) · N. Tanigawa · S. Kariya · H. Kojima · Y. Shomura · T. Tokuda · M. Nomura · J. Terada · M. Kamata · S. Sawada
Department of Radiology, Kansai Medical University, 2-3-1 Shinmachi, Hirakata, Osaka 573-1191, Japan
e-mail: kome64@yo.rim.or.jp

Introduction

Percutaneous vertebroplasty is used to treat back pain caused by compression fractures. Injecting bone cement into fractured vertebral bodies increases the strength and stability of vertebral body bone, which is thought to be a factor in alleviation of pain [1–3]. Several studies indicate that new fractures can occur following percutaneous vertebroplasty [4–7]. Osteoporosis, which is a skeletal disorder characterized by decreased bone strength that increases the risk of fracture, affects the occurrence of new fractures after vertebroplasty [3–5]. Bone strength is determined by bone mineral density and bone quality [8]. Bone quality is determined by characteristics of the bone matrix, such as microarchitecture, bone turnover, microdamage accumulation, the degree of calcification, and collagen [9, 10]. Currently, it is thought that the only reliable way to clinically assess bone quality is to characterize bone metabolism by assaying biochemical markers of bone turnover [8]. The present study evaluated relationships between biochemical markers of bone turnover, bone mineral density, and new compression fractures following vertebroplasty.

Patients and Methods

This study was approved by our Institutional Review Board. All patients received explanations of the

percutaneous vertebroplasty and the handling of clinical data, and written informed consent was obtained from each patient. There was no financial relationship between the investigators and the study subjects.

Initially, we enrolled 30 consecutive patients with vertebral body compression fractures caused by osteoporosis. All patients underwent percutaneous vertebroplasty at a single institution from January 2005 to December 2005. Patients with traumatic compression fracture or malignant tumors were excluded from this study. The latest clinical data we used were obtained in September 2006. Twenty-three of the 30 patients visited our hospital for follow-up examinations for more than 4 weeks after vertebroplasty (mean follow-up term, 255.0 ± 173.1 days; median follow-up term, 275.5 days; range, 31–591 days). These 23 patients (21 women, 2 men; mean age, 72.1 ± 6.7 years; age range, 63–86 years), encompassing 48 vertebral body compression fractures (Th6, 1; Th7, 3; Th8, 2; Th9, 4; Th10, 3; Th11, 8; Th12, 6; L1, 7; L2, 4; L3, 9; L4, 1), and 26 percutaneous vertebroplasty procedures, were the subjects of this study.

The indication for vertebroplasty was compression fracture causing significant back pain that was not relieved by conservative treatment. Patients underwent the following numbers of vertebroplasty procedures: one procedure, 20 patients; two procedures, 3 patients. Before each vertebroplasty procedure, we measured serum bone alkaline phosphatase, urinary crosslinked N-telopeptide of type I collagen, urinary deoxypyridinoline, and bone mineral density. Bone mineral density of the second metacarpal bone was measured by computed X-ray densitometry (Bonalyzer II, Teijin, Tokyo, Japan), and the quantity ΣGS/D (mmAl) was used for analysis.

Percutaneous vertebroplasty was performed in an angiography room with an IVR-CT system (Advantex LCA + ACT, GE Medical Systems, Milwaukee, WI, USA), which combines angiographic equipment and CT equipment with a single fluoroscopy table. After intramuscular injection of 25 mg of hydroxyzine hydrochloride (Atarax P, Pfizer Japan, Tokyo, Japan), 0.5 mg of atropine sulfate (Tanabe Seiyaku, Osaka, Japan) and 10 mg of morphine hydrochloride (Sankyo, Tokyo, Japan), the patient was placed prone on the fluoroscopy table. The skin, subcutaneous tissues, and periosteum over the pedicle to be punctured were anesthetized with 1% lidocaine hydrochloride (Xylocaine polyamp 1%, AstraZeneca, Osaka, Japan). A 13G needle (Osteo-Site Bone Biopsy Needle Murphy M2; length, 10 cm; Cook, Bloomington, IN, USA) was advanced until its tip penetrated the cortex, with reference to CT images. With lateral fluoroscopic guidance, the needle was advanced into the vertebral body. Ideally, the tip of the needle was placed in the anterior third of the vertebral body, close to the midline. More posterior needle positions were sometimes necessary when treating severely compressed vertebral bodies with steep pedicle angulation.

Intraosseous venography was performed with 10–20 ml of CO_2 to confirm that the needle was not positioned within a direct venous anastomosis to the central or epidural veins [11]. Then, 20 g of methylmethacrylate powder (Osteobond copolymer bone cement; Zimmer, Warsaw, IN, USA) was mixed with 5 g of barium sulfate powder (Horii Pharmaceutical, Osaka, Japan) that had been sterilized with dry heat to increase its opacity [12]. Next, 10 ml of liquid methylmethacrylate monomer was added to the powder, and the mixture was blended to a toothpaste-like consistency, producing polymethylmethacrylate (PMM). Using 1 ml syringes, the PMM was injected with lateral fluoroscopic guidance. PMM injection was terminated when adequate filling of the vertebral body was achieved, or if leakage occurred. If leakage occurred, the needle was repositioned, and additional PMM was injected to fill the remaining part of the vertebral body. After the needle was removed, all patients were observed in a supine position for 2 hr.

After the vertebroplasty, the patients were followed up with physical examinations and radiographs at 1 to 3 days and 1, 4, 10, and 22 months after vertebroplasty, and if back pain relapsed. If a patient did not visit the hospital for follow-up, a physician telephoned them to encourage them to visit. Even if no new fractures were observed on radiographs, MRI was performed to check for microfractures or incomplete fractures if new fractures were suspected on physical examination. MRI was performed using a 1.5 T MRI system (Signa Horizon LX software version 9.1; General Electric Medical Systems, Milwaukee, WI, USA) and a phased-array cervico-thoraco-lumbar coil. At all MRI examinations, images were acquired using the following procedures: T1-weighted fast gradient echo (TR, 10 msec; TE, 4 msec; flip angle, 30°); sagittal T1-weighted spin echo (TR, 500 msec; TE, 9 msec; excitations, 4; matrix, 384 × 256); and sagittal T2-weighted fast spin echo with fat suppression (TR, 4000 msec; TE, 102 msec; excitations, 2; matrix, 320 × 256). Additional imaging procedures were performed if necessary. The criteria for diagnosis of vertebral fracture were deformation of the vertebral body on plain radiographs and a change in vertebral signal intensity on MRI [13]. We recommended to all patients that they be administered vitamin D or antiresorptive agents by their family doctor.

The patients were divided into two groups: patients with new fractures (group F) and patients with no new fractures (group N). Using Student's *t*-test, we analyzed differences in the following parameters between these two groups: serum bone alkaline phosphatase, urinary crosslinked N-telopeptide of type I collagen, urinary deoxypyridinoline, and bone mineral density.

Next, the patients were divided into another two groups: patients with higher risk of fracture (group H) and patients with lower risk of fracture (group L). Group H was defined according to guidelines for the use of biochemical markers of bone turnover in osteoporosis [8]: urinary crosslinked N-telopeptide of type I collagen >54.3 nmol BCE/mmol Cr or urinary deoxypyridinoline >7.6 nmol/mmol Cr; and serum bone alkaline phosphatase <29.0 U/l. Using the chi-square test, we analyzed the difference in the rate of new fractures between group H and group L.

A probability value of $p < 0.05$ was considered significant. All analyses were performed using StatView for Windows (version 5.0, SAS Institute, Cary, NC, USA).

Results

We identified 9 new fractures in 7 (30%) of the 23 patients. These 7 patients comprised group F. The remaining 16 patients (70%) comprised group N.

In group F and group N, respectively, serum bone alkaline phosphatase was 30.1 ± 15.3 and 25.3 ± 8.6 U/l, urinary crosslinked N-telopeptide of type I collagen was 63.9 ± 33.2 and 50.7 ± 29.2 nmol BCE/mmol Cr, urinary deoxypyridinoline was 8.4 ± 2.9 and 7.3 ± 3.3 nmol/mmol Cr, and bone mineral density was 2.2 ± 0.2 and 2.0 ± 0.3 mmAl. There were no significant differences in bone mineral density or any of the biochemical markers of bone turnover that we evaluated between group F and group N (Table 1). There was no significant difference in age, gender, locations, and activity after initial vertebroplasty between group F and group N.

Group H comprised 4 (17%) of the 23 patients, and group L comprised the remaining 19 patients (83%). We identified 5 new fractures in 3 (75%) of the 4 patients in group H, and 4 new fractures in 4 (21%) of the 19 patients in group L. There was a significant difference in the rate of new fractures between group H and group L (chi-square test: $p = 0.03$) (Table 2). There was no significant difference in age, gender, locations, and activity after initial vertebroplasty between group H and group L.

Table 2 Comparison of occurrence of new fractures between group H (high fracture risk) and group L (low fracture risk)

	New fractures	No new fractures	Total
Group H ($n = 4$)	3	1	4
Group L ($n = 19$)	4	15	19
Total	7	16	23

Group H: urinary crosslinked N-telopeptide of type I collagen >54.3 nmol BCE/mmol Cr or urinary deoxypyridinoline > 7.6, and serum bone alkaline phosphatase < 29.0 U/l

Chi-square test: $p = 0.03$

Discussion

There have been reports of new vertebral fractures following percutaneous vertebroplasty [4–6]. New vertebral fractures are 5 times more likely to occur in patients with compression fractures caused by osteoporosis, but it is unclear whether these fractures are due to the natural history of osteoporosis or the effects of vertebroplasty [14, 15]. When following patients after percutaneous vertebroplasty, it is important to be able to predict the risk of new vertebral fractures. It is thought that various factors are involved in the occurrence of new fractures after vertebroplasty [16]. In the present study, we examined relationships between bone mineral density, biochemical markers of bone turnover, and new fractures after vertebroplasty.

In several previous studies of new fractures after vertebroplasty [5, 6], follow-up examinations were performed when symptoms recurred; consequently, researchers were unable to detect asymptomatic vertebral fractures. In the present study, the patients were followed whether or not symptoms recurred, allowing us to identify asymptomatic vertebral fractures. Furthermore, whereas incomplete fractures are difficult to identify on spine radiographs, they can easily be seen on MRI scans. In a previous study, 67% of new compression fractures following percutaneous vertebroplasty occurred within 30 days after the surgery [5]. In the present study, we found 9 new fractures in 7 (30%) of the 23 consecutive patients, who were followed

Table 1 Comparison of the following parameters between groups F (new fractures) and N (no new fractures): serum bone alkaline phosphatase, urinary crosslinked N-telopeptide of type I collagen, urinary deoxypyridinoline, and bone mineral density

	Group F ($n = 7$)	Group N ($n = 16$)	Student's t-test
Serum bone alkaline phosphatase (U/l)	30.1 ± 15.3	25.3 ± 8.6	NS
Urinary crosslinked N-telopeptide of type I collagen (nmol BCE/mmol Cr)	63.9 ± 33.2	50.7 ± 29.2	NS
Urinary deoxypyridinoline (nmol/mmol Cr)	8.4 ± 2.9	7.3 ± 3.3	NS
Bone mineral density (mmAl)	2.2 ± 0.2	2.0 ± 0.3	NS

for more than 4 weeks, with an average follow-up period of 255.0 days.

As the bone mineral density of trunk bones can be affected by compression fractures or bone cement, the bone mineral density of the second metacarpal bone was measured in this study. Previous meta-analysis of bone mineral density and risk of vertebral fractures indicates that the confidence intervals for estimates of relative risk of new vertebral fractures are relatively wide in the great majority of trials. The meta-analysis showed that a 1% improvement in bone mineral density was associated with a 0.03 decrease in the relative risk of vertebral fractures, and indicated that the status of bone resorption is more predictive than bone mineral density [17]. In the present study, serum bone alkaline phosphatase was measured as a bone formation marker. Bone formation markers are directly or indirectly produced by osteoblasts during bone development [8]. In the present study, urinary crosslinked N-telopeptide of type I collagen and urinary deoxypyridinoline were measured as bone resorption markers. Bone resorption markers are produced by osteoclasts during bone resorption, and a decrease in these markers indicates a reduction in the risk of fracture [8]. We did not find any differences in any of the biochemical markers of bone turnover or bone mineral density between group F and group N.

According to the Japan Osteoporosis Society's Guidelines, a combination of high levels of bone resorption markers and normal levels of bone formation markers is associated with a higher risk of fracture [8]. We divided the present patients into two groups: higher risk of fracture (group H) and lower risk of fracture (group L). Group H was defined according to guidelines for the use of biochemical markers of bone turnover in osteoporosis: urinary crosslinked N-telopeptide of type I collagen >54.3 nmol BCE/mmol Cr or urinary deoxypyridinoline >7.6 nmol/mmol Cr, and serum bone alkaline phosphatase <29.0 U/l. Group H had a significantly higher incidence rate of fracture than group L.

The present study had the following limitations: the study group comprised a relatively small number of patients (in particular there were only 4 patients in group H) treated at a single institution, and subjects received antiresorptive drugs or vitamin D that were administered by their family doctor which were not controlled by the researchers.

In conclusion, this single-center feasibility study suggests a relationship between high levels of bone resorption markers and normal levels of bone formation markers and an increased risk of new recurrent fractures after percutaneous vertebroplasty. These findings may warrant validation a larger prospective multicenter study.

References

1. Cotten A, Boutry N, Cortet B et al. (1998) Percutaneous vertebroplasty: State of the art. Radiographics 18:311–323
2. Peh WC, Gilula LA, Peck DD (2002) Percutaneous vertebroplasty for severe osteoporotic vertebral body compression fractures. Radiology 223:121–126
3. Kallmes DF, Jensen ME (2003) Percutaneous vertebroplasty. Radiology 229:27–36
4. Grados F, Depriester C, Cayrolle G et al. (2000) Long-term observations of vertebral osteoporotic fractures treated by percutaneous vertebroplasty. Rheumatology (Oxford) 39:1410–1414
5. Uppin AA, Hirsch JA, Centenera LV et al. (2003) Occurrence of new vertebral body fracture after percutaneous vertebroplasty in patients with osteoporosis. Radiology 226:119–124
6. Lin EP, Ekholm S, Hiwatashi A et al. (2004) Vertebroplasty: Cement leakage into the disc increases the risk of new fracture of adjacent vertebral body. AJNR Am J Neuroradiol 25:175–180
7. Komemushi A, Tanigawa N, Kariya S et al. (2006) Percutaneous vertebroplasty for osteoporotic compression fracture: Multivariate study of predictors of new vertebral body fracture. Cardiovasc Intervent Radiol 29:580–585
8. Nishizawa Y, Nakamura T, Ohta H et al. (2005) Guidelines for the use of biochemical markers of bone turnover in osteoporosis (2004). J Bone Miner Metab 23:97–104
9. Weinstein RS (2000) True strength. J Bone Miner Res 15:621–625
10. Chesnut CH 3rd, Rosen CJ, Bone Quality Discussion Group (2001) Reconsidering the effects of antiresorptive therapies in reducing osteoporotic fracture. J Bone Miner Res 16:2163–2172
11. Tanigawa N, Komemushi A, Kariya S et al. (2005) Intraosseous venography with carbon dioxide contrast agent in percutaneous vertebroplasty. AJR Am J Roentgenol 184:567–570
12. Leibold RA, Gilula LA (2002) Sterilization of barium for vertebroplasty: An effective, reliable, and inexpensive method to sterilize powders for surgical procedures. AJR Am J Roentgenol 179:198–200
13. Maehara M, Tanigawa N, Ikeda K et al. (2006) Gadolinium-enhanced magnetic resonance imaging after percutaneous vertebroplasty does not improve the short-term prediction of new compression fractures. Acta Radiol 47:817–822
14. Lindsay R, Silverman SL, Cooper C et al. (2001) Risk of new vertebral fracture in the year following a fracture. JAMA 285:320–323
15. Delmas PD, Ensrud KE, Adachi JD et al. (2002) Multiple Outcomes of Raloxifene Evaluation Investigators. Efficacy of raloxifene on vertebral fracture risk reduction in postmenopausal women with osteoporosis: Four-year results from a randomized clinical trial. J Clin Endocrinol Metab 87:3609–3617
16. Hulme PA, Krebs J, Ferguson SJ et al. (2006) Vertebroplasty and kyphoplasty: A systematic review of 69 clinical studies. Spine 31:1983–2001
17. Cummings SR, Karpf DB, Harris F et al. (2002) Improvement in spine bone density and reduction in risk of vertebral fractures during treatment with antiresorptive drugs. Am J Med 112:281–289

ORIGINAL ARTICLE

ACTA RADIOLOGICA

Diffusion-Weighted Imaging for Predicting New Compression Fractures Following Percutaneous Vertebroplasty

T. SUGIMOTO, N. TANIGAWA, K. IKEDA, N. OHMURA, M. MAEHARA, S. KARIYA, H. KOJIMA, A. KOMEMUSHI, S. K. HA-KAWA, Y. SAITO, A. TAJIKA, T. KINOSHITA & S. SAWADA

Department of Radiology and Department of Neuropsychiatry, Kansai Medical University Takii Hospital, Osaka, Japan; Department of Radiology, Kansai Medical University, Osaka, Japan

Sugimoto T, Tanigawa N, Ikeda K, Ohmura N, Maehara M, Kariya S, Kojima H, Komemushi A, Ha-Kawa SK, Saito Y, Tajika A, Kinoshita T, Sawada S. Diffusion-weighted imaging for predicting new compression fractures following percutaneous vertebroplasty. Acta Radiol 2008;49:419–426.

Background: Percutaneous vertebroplasty (PVP) is a technique that structurally stabilizes a fractured vertebral body. However, some patients return to the hospital due to recurrent back pain following PVP, and such pain is sometimes caused by new compression fractures.

Purpose: To investigate whether the apparent diffusion coefficient (ADC) of adjacent vertebral bodies as assessed by diffusion-weighted imaging before PVP could predict the onset of new compression fractures following PVP.

Material and Methods: 25 patients with osteoporotic compression fractures who underwent PVP were enrolled in this study. ADC was measured for 49 vertebral bodies immediately above and below each vertebral body injected with bone cement before and after PVP. By measuring ADC for each adjacent vertebral body, ADC was compared between vertebral bodies with a new compression fracture within 1 month and those without new compression fractures. In addition, the mean ADC of adjacent vertebral bodies per patient was calculated.

Results: Mean preoperative ADC for the six adjacent vertebral bodies with new compression fractures was 0.55×10^{-3} mm^2/s (range 0.36–1.01×10^{-3} mm^2/s), and for the 43 adjacent vertebral bodies without new compression fractures 0.20×10^{-3} mm^2/s (range 0–0.98×10^{-3} mm^2/s) ($P < 0.001$). Mean preoperative ADC for the six patients with new compression fractures was 0.55×10^{-3} mm^2/s (range 0.21–1.01×10^{-3} mm^2/s), and that for the 19 patients without new compression fractures 0.17×10^{-3} mm^2/s (range 0.01–0.43×10^{-3} mm^2/s) ($P < 0.001$).

Conclusion: The ADC of adjacent vertebral bodies as assessed by diffusion-weighted imaging before PVP might be one of the predictors for new compression fractures following PVP.

Key words: Adults; CNS; MR diffusion; spine; vertebroplasty

Tatsuya Sugimoto, Department of Radiology and Neuropsychiatry, Kansai Medical University Takii Hospital, 10–15 Fumizono, Moriguchi, Osaka, 570-8507, Japan (tel. +81 6 6992 1001, fax. +81 6 6995 2669, e-mail. sugimota@takii.kmu.ac.jp)

Accepted for publication December 6, 2007

Percutaneous vertebroplasty (PVP) was introduced into the literature in 1987 (1). Since then, PVP has been performed to treat back pain associated with vertebral body compression fractures caused by various factors, and is now widely performed due to its drastic pain-relieving effects. PVP is a technique that structurally stabilizes a fractured vertebral body by injecting a self-curing cement substance that uses polymethyl methacrylate (PMMA) as the main component. However, some patients return to the hospital due to recurrent back pain following PVP. Such pain is sometimes caused by new compression fractures. While general consensus is lacking regarding the causes of new compression fractures following PVP, new fractures often occur in vertebral bodies adjacent to the vertebral bodies treated by PVP (2–4). Furthermore, such new compression fractures occur relatively

informa
healthcare

DOI 10.1080/02841850801886109

soon after PVP (4). If new adjacent-level compression fractures can be predicted prior to PVP, use of prophylactic PVP in adjacent vertebral bodies may be justified (5–9).

In recent years, many studies have investigated the differentiation between benign and malignant compression fractures using diffusion-weighted magnetic resonance imaging (MRI) (10–14). Diffusion-weighted imaging (DWI) allows visualization of the diffusion of water molecules exhibiting random and Brownian motions in tissue, and ascertainment of microscopic findings for cells. Furthermore, measuring the apparent diffusion coefficient (ADC) allows objective assessment of diffusion. In an attempt to establish the possibility of prophylactic PVP, the present study examined vertebral bodies adjacent to vertebral bodies injected with bone cement substance, based on the hypothesis that adjacent vertebrae are at high risk of compression fractures. The purpose of this study was to ascertain whether the ADC of adjacent vertebral bodies as assessed by diffusion-weighted imaging prior to PVP could predict the onset of new compression fractures following PVP.

Material and Methods

This study was approved by the institutional review board. All patients provided written informed consent.

Patients

The subjects in this study comprised 31 (27 female, four male; mean age 71.2±8.4 years, range 44–84 years) consecutive patients who underwent PVP for vertebral compression fractures resulting from osteoporosis between April and July 2003. Indication for PVP was back pain caused by compression fracture of a vertebral body with pain on percussion of the vertebral spinous process. In cases with multiple compression fractures in which percussion pain of spinous process was unclear, physical examination was performed using fluoroscopy. Patients with back pain attributed to myelopathy or radiculopathy resulting from stenosis of the vertebral canal or narrowing of the intervertebral foramen were excluded from the present study. Examinations performed before the procedure comprised physical and neurological examinations, electrocardiography, respiratory function testing, laboratory investigations, evaluation of back pain using visual analogue scale (VAS) score and the following diagnostic imaging studies: anterior and lateral radiographs of the thoracic and lumbar vertebrae, MRI of the spine, including the vertebra affected by the compression fracture, and computed tomography (CT).

ADC was measured for the vertebral bodies immediately above and below each vertebral body injected with bone cement. Inclusion and exclusion criteria were as follows. Vertebrae placed just below and above the treated vertebrae and where ADC could be accurately calculated were included in our study. The following vertebrae were excluded: vertebrae injected with bone cement after initial PVP within 1 month; first sacrum (S1); fractured vertebrae; vertebrae with susceptibility artifacts. A patient summary, including excluded patients, is shown in Table 1.

PVP was performed on 69 vertebral bodies. Six patients were excluded due to the reasons listed in Table 1. The remaining 25 patients (22 female, three male; mean age 72.2±6.5 years, range 54–84 years) were included in the final analysis. A total of 56 vertebral bodies (20 thoracic vertebral bodies and 36 lumbar vertebral bodies) were treated by PVP in these 25 patients. The number of treated vertebral bodies was one in seven patients, two in seven patients, three in nine patients, and four in two patients. Among the 18 patients in whom cement injection was performed in multiple vertebral bodies, the number of normal vertebral bodies between treated vertebral bodies was zero in nine patients, one in three patients, two in five patients, and three in one patient. Thus, excluding S1, a total of 62 adjacent vertebral bodies were examined. Of the 62 vertebral bodies, four vertebral bodies with compression fractures identified at the time of PVP and nine vertebral bodies in which ADC could not be measured due to susceptibility artifacts were excluded. ADC was thus measured in 49 vertebral bodies (16 thoracic vertebral bodies, 33 lumbar vertebral bodies).

MR imaging protocol

MRI was performed using a 1.5T MRI system (Signa Horizon LX software version 9.1; GE HealthCare, Milwaukee, Wisc., USA) within 3 days before PVP and within 1 week after PVP. A quadrature detection thoracolumbar spine coil was used for T1- and T2-weighted imaging and DWI. Following T1-weighted fast gradient-echo coronal localizer images, sagittal T1-weighted spin-echo (TR/TE 675/12 ms, slice thickness 3.7 mm, intersection gap 0.8 mm, field of view [FOV] 30 × 30 cm, matrix size 384 × 256, echo train length 4) and sagittal T2-weighted fast spin-echo with fat suppression (TR/TE 4000/102 ms, slice thickness 3.7 mm,

Table 1. Patient data.

Patient	Sex	Age, years	PVP performed on vertebral bodies	Adjacent vertebral bodies	Analyzed vertebral bodies	Reason for analysis exclusion
A	M	76	L2, L3	L1, L4	L1, L4	
B	F	66	TH12, L1, L2, L3	Th11, L4	Th11, L4	
C	F	74	Th11, Th12, L1	Th10, L2	Th10, L2	
D	F	76	Th6, Th8	Th5, Th7, Th9	Th9	Th5: artifacts Th7: artifacts
E	F	79	Th12	Th11, L1	Th11, L1	
F	M	66	L1	Th12, L2	Th12, L2	
G	M	54	L1	Th12, L2	Th12, L2	
H	F	70	Th12	Th11, L1	Th11, L1	
I	F	69	Th12, L1, L2	Th11, L3	Th11, L3	
J	F	64	L1, L2	Th12, L3	L3	Th12: artifacts
K	F	80	Th12, L3	Th11, L1, L2, L4	L1	Th11: artifacts L2: compression fracture L4: compression fracture
L	F	76	L1, L4	Th12, L2, L3, L5	L2, L3, L5	Th12: artifacts
M	F	69	Th12, L1, L3	Th11, L2, L4	L2, L4	Th11: artifacts
N	F	72	L3	L2, L4	L2, L4	
O	F	70	L4, L5	L3	L3	
P	F	71	L1, L2, L3	Th12, L4	Th12, L4	
Q	F	84	L3	L2, L4	L2, L4	
R	F	76	Th11, Th12, L1, L2	Th10, L3	Th10	L3: compression fracture
S	F	78	L1, L4, L5	Th12, L2, L3	Th12, L2, L3	
T	F	63	Th12	Th11, L1	Th11, L1	
U	F	79	Th11, Th12, L3	Th10, L1, L2, L4	L1, L2, L4	Th10: artifacts
V	F	71	Th12, L4, L5	Th11, L1, L3	Th11, L3	L1: compression fracture
W	F	71	Th12, L1, L3	Th11, L2, L4	Th11, L2, L4	
X	F	78	Th9, Th12, L1	Th8, Th10, Th11, L2	Th11, L2	Th8: artifacts Th10: artifacts
Y	F	74	Th12, L1	Th11, L2	Th11, L2	
($n=25$)	3 M, 22 F	72.2±6.5	56 (20 Th, 36 L)	62 (25 Th, 37 L)	49 (16 Th, 33 L)	13 (9 Th, 4 L)
Excluded patients						
a	M	84	L3, L4, L5			L2: compression fracture
b	F	59	L3, L4, L5			Additional PVP was performed 6 days after initial PVP
c	F	74	L2			Additional PVP was performed 6 days after initial PVP
d	F	72	Th12			Th11 and L1: artifact
e	F	69	Th11, Th12			Additional PVP was performed 7 days after initial PVP
f	F	44	Th10, Th11, Th12			Th9 and L1: compression fracture
($n=6$)			13 (3 Th, 7 L)			

intersection gap 0.8 mm, FOV 30 × 30 cm, matrix size 320 × 256, echo train length 16) images were acquired. The MR pulse sequence used for DWI was a single-shot echo-planar pulse sequence with fat saturation (TR/TE 5000/99.1 ms, receiver bandwidth ±108 kHz, FOV 30 × 30 cm, matrix size 128 × 128, slice thickness 8 mm, interslice gap 2 mm, number of excitations [NEX] 1). Using these parameters, seven sagittal diffusion-weighted images were acquired.

ADCs were calculated with only two b factors (0 s/mm^{-2}, 1000 s/mm^{-2}) (two-point technique) (15).

Data from DWI were transferred to a GE Advantage Workstation 3.1, where ADCs were calculated using a subprogram of the Functool2 image analysis software (GE HealthCare, Buc, France). A user-defined region of interest (ROI) was placed in the mid-sagittal diffusion-weighted image. On the target vertebral bodies, the large

fitting circle or ellipse was positioned centrally (Fig. 1). Special care was taken to avoid cerebrospinal fluid signal or vertebral disk signal. The average ADC within the ROI calculated by Functool2 was presumed to be the mean ADC of the target vertebral body.

Follow-up protocol and outcome evaluation

Frontal and lateral radiographs of the thoracic and lumbar vertebrae were performed within 3 days of PVP (baseline). At 1 month after PVP, a frontal and lateral radiograph of the thoracic and lumbar vertebrae was performed, in addition to MRI. Subjects were instructed to return to the hospital if back pain recurred within 1 month of PVP, and frontal and lateral radiographs of the thoracic and lumbar vertebrae and MRI were taken at this point in time. VAS was used for the evaluation of back pain. New compression fractures were defined as follows: localized spontaneous pain and pain on percussion of the vertebral spinous process, a bone marrow edema pattern as assessed by MRI, and reduced vertebral height on radiography. Two radiologists independently reviewed imaging findings, and if their opinions did not agree, the final diagnosis was determined after consultation between both radiologists.

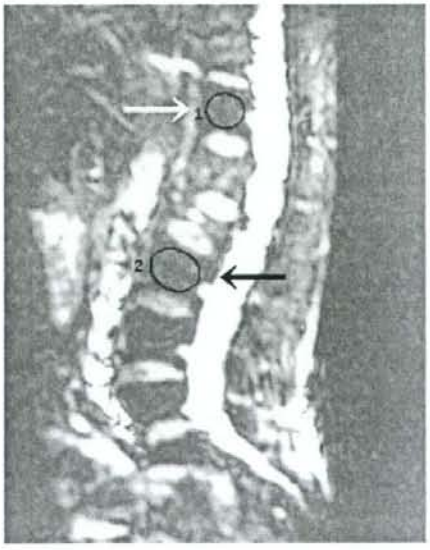

Fig. 1. User-defined ROI. Mid-sagittal diffusion-weighted image before PVP in a 64-year-old woman with L1 and L2 compression fractures. Two days after, PVP was performed on L1 and L2, so target vertebral bodies were Th12 and L3. The large fitting circle and ellipse were positioned centrally on Th12 and L3 (arrow).

Evaluated items and statistics

Relationships between preoperative ADC and new compression fractures were examined from two perspectives. By measuring ADC for each adjacent vertebral body, the ADC of vertebral bodies with a new compression fracture within 1 month and those without a new compression fracture was compared. In addition, mean ADC of adjacent vertebral bodies per patient was calculated, and ADC of patients with new compression fractures within 1 month and patients without new compression fractures was compared. Furthermore, changes in ADC before and after PVP were examined. In cases with one adjacent vertebra that met with inclusion criteria, the ADC of the vertebra was used as the mean ADC of adjacent vertebral bodies, and with more than one more adjacent vertebra, the mean ADC of the adjacent vertebrae was used.

Two-sample t tests were used to compare ADCs between vertebral bodies with new compression fractures within 1 month of PVP and those without, and to compare ADCs between patients with new compression fractures within 1 month of PVP and those without. One-sample t tests were used to compare ADCs before and after PVP. Values of $P < 0.05$ were considered statistically significant.

Results

Within 1 month of PVP, a new compression fracture had developed in seven vertebral bodies in seven of the 25 patients (28.0%). Of the seven new fractures, six were adjacent-level fractures (24%), while one was a non-adjacent-level fracture (4%). No new compression fractures were seen within 1 month of PVP in the other 18 patients (Table 2).

Mean preoperative ADC for the six adjacent vertebral bodies with new compression fractures was 0.55×10^{-3} mm^2/s (range 0.36–1.01 $\times 10^{-3}$ mm^2/s), and that of the 43 adjacent vertebral bodies without new compression fractures 0.20×10^{-3} mm^2/s (range 0–0.98 $\times 10^{-3}$ mm^2/s). This difference was statistically significant ($P < 0.001$; Fig. 2). Mean preoperative ADC for the six patients with new compression fractures was 0.55×10^{-3} mm^2/s (range 0.21–1.01 $\times 10^{-3}$ mm^2/s), and that for the 19 patients without new compression fractures 0.17×10^{-3} mm^2/s (range 0.01–0.43 $\times 10^{-3}$ mm^2/s). A statistically significant difference was again identified between the two groups ($P < 0.001$; Fig. 3).

Mean ADC for adjacent vertebral bodies was 0.24×10^{-3} mm^2/s (range 0–1.01 $\times 10^{-3}$ mm^2/s)